Jha and Malgwi
*Journal of the Egyptian Mathematical Society* (2022) 30:21
https://doi.org/10.1186/s42787-022-00155-w

Journal of the Egyptian Mathematical Society

ORIGINAL RESEARCH Open Access

# Hydromagnetic free convection flow in a vertical microporous channel with Hall current and ion-slip effect

Basant K. Jha[1] and Peter B. Malgwi[2*]

*Correspondence: bumalpeter@gmail.com

[1] Department of Mathematics, Ahmadu Bello University, Zaria, Nigeria
[2] Department of Mathematics, Air Force Institute of Technology, Kaduna, Nigeria

**Abstract**

In the present work, steady-state hydromagnetic analysis and flow formation of Newtonian viscous fluid through a vertical microporous channel is studied theoretically. The transport governing equations include the effect of Hall current and ion-slip effects in the microchannel slip regime. Unlike the usual employed thermal properties of constant heat flux/temperature at the boundary, the current work assumes that the microporous walls are influenced by different surrounding wall temperatures. Solution to the governing equations depending on Prandtl number, rarefaction parameter, Hall current parameter, ion-slip parameter, Hartmann number and suction/injection parameter are obtained by utilizing the method of undetermined coefficient. Results demonstrating the effect of these parameters on different flow features are presented graphically in MATLAB. The results reveal that in the simultaneous occurrence of Hall and ion-slip currents, higher values of rarefaction parameter enhance the momentum boundary layer in both primary and secondary flow directions. In addition, results from this analysis also reveal that the main component of fluid velocity remains unaffected to higher values of Hall current, whereas it decreases along the induced flow directions. Furthermore, for a specific value of Hall parameter and ion-slip current, injection weakens the buoyancy drive resulting in a reduction in volume flow rate. The contrast is true with suction.

**Keywords:** Free convection, Microporous channel, Hall current, Ion-slip, Velocity slip, Temperature jump

## Introduction

Hydromagnetic flow in microchannels is important owing to new advances in technological applications like magneto-plasma dynamics (MPD) thrusters, boundary layer heat transfer, micro-chip cooling, microelectromechanical systems (MEMS), nano-electromechanical systems (NEMS) and biochemical cell reaction. These flows are also encountered in many nuclear thermohydraulic processes and magnetohydrodynamic energy systems. Studies relating to this type of flows are important to improve the efficiency of these devices. Owing to its widespread applications, the groundbreaking work of Hartmann [1] leads to several studies on hydromagnetic free convection flows both theoretically and experimentally. Few among them include the following: Jha and Aina

[2] illustrated the impact of magnetic field applied transversely and mixed convection current on MHD flow of conducting fluid through a microchannel in the occurrence of induced magnetic field. Jha and Aina [3], in a recent study, extended their work to the situation when one of the microchannel walls is assumed to be electrically conducting. Jha and Aina [4] also examined the influence of induced magnetic field on MHD free convection past an insulated vertical microchannel. Other notable works on MHD flow are as follows: Chandran et al. [5] analyzed the flow of viscous incompressible and electrically conducting fluid in a porous channel with magnetic and heat transfer effects. In a connected work, Chandran et al. [6] extended their study to investigate the effect of constant heat flux and accelerated movement of the boundary walls. Jha and Apere [7] investigated on hydromagnetic flow of viscous incompressible fluid past a permeable channel due to sudden impulsive motion.

It is challenging to observe that in most of the reported literature, the occurrence of Hall current in the magnetohydrodynamic flow equations has been neglected. These assumptions become feasible for low magnetic field strength. As reported by Cowling [8], it becomes relevant to note that in the instance when the magnetic field is taken to be strong, the effect of Hall current befits its significance and should not be neglected. Some studies on the above subject include the following: Singh [9] examined the hydromagnetic flow of conducting fluid due to buoyancy force in the presence of Hall current and observed that cooling the permeable wall supports flow formation in the presence Hall current, while the contrast is displayed for heating. Seth and Ansari [10], in their analysis, reported the impact of Hall current on free conductive flow of conducting fluid past a rotating system. Seth and Singh [11] also reported the impact of Hall current on hydromagnetic convective flow in the occurrence of constant pressure past a conducting/insulated revolving system. They established that in the occurrence of Hall current, a rise in rotation weakens the main flow velocity, while the contrast is revealed toward the induced flow direction. Attia [12] offered an investigation on unsteady viscous flow in the occurrence of Hall current and heat transfer effects. It was observed that Hall parameter strengthens the impact of magnetic field on both main flow and induced flow velocity profiles. Recently, Jha et al. [13] studied the impact of Hall current on hydromagnetic convective flow of viscous fluid past a microchannel with different surrounding temperatures. They found out that Hall current aids flow formation along main flow direction for both symmetric and asymmetric heating. Other articles on the above subject under different geometric situations are as follows: Ram [14], Ali et al. [15], Makinde et al. [16], Krishna and Jyothi [17], Jha and Apere [18, 19], Mazumder et al. [20], Ghosh [21], Jha and Malgwi [22] and Seth and Singh [23].

In a connected work, Zhang et al. [24] investigated the influence of induced magnetic field on hybrid nanofluid flow of viscous incompressible and electrically conducting fluid near an elastic surface. Electroosmotic flow of non-Newtonian fluid in a microchannel in the occurrence of nanoparticles has been investigated by Bhatti et al. [25]. Analysis of non-local nanobeams incorporating the Euler–Bernoulli and modified coupled stress theory has been discussed by Abouelregal and Marin [26]. Ghita et al. [27] formulated some models by utilizing the local hardening behavior of a plastic material following the Prandtl–Reuss law. In a related work, Anwar et al. [28] discussed enhancement in radiative heat transfer of hydromagnetic flow of Oldroyd-B fluid in a porous channel under

generalized boundary conditions. Other relevant works include Bratu et al. [29], Marin et al. [30] and Jha et al. [34].

In all the above-reported literature studies, none considered the combined effects of Hall current and ion-slip influence on hydromagnetic convective flow involving a viscous fluid through a permeable microchannel subject to symmetric/asymmetric surrounding wall surface temperatures. Studies relating to these flows have found relevance in the field of fluid engineering and other manufacturing industries and have not been accounted for in the open literature, which is the motivation of this work. Jha et al. [31] investigated the influence of transversely applied magnetic field on natural convection flow of Newtonian viscous fluid in a vertical microporous channel heated asymmetrically. The present work is an extension of the work of Jha et al. [31] by incorporating the combined influence of Hall and ion-slip current in the presence of simultaneous suction/injection on steady hydromagnetic flow of conducting viscous fluid in a vertical microchannel. Hence, the main objective of this work is to present a theoretical analysis on influence of Hall and ion-slip current in a vertical microporous channel with asymmetrical thermal boundary conditions. It is well established that analytical solutions have their own theoretical meaning and play a vital role in the early development of many fluid mechanics and heat transfer problems. Furthermore, theoretical analysis could be useful in validating the accuracy and convergence and improving the effectiveness of most numerical computation and experimental analysis. As stated earlier, the impact of Hall current in the occurrence of ion-slip current becomes significant when the influence of the applied magnetic field becomes large, thereby inducing secondary flow. Effects of flow parameters on velocity, volume flow rate, skin friction and volume flow rate are examined.

## Method

Consider the one-dimensional buoyancy-driven flow of viscous incompressible and electrically conducting fluid through a vertical microchannel. The microchannel walls are assumed to be porous and heated with different surrounding wall temperatures. The impact of Hall and ion slip are included in the flow equations. The $x'$-coordinate is taken along the walls, ascending vertically upward, whereas the $y'$-coordinate is measured perpendicular to the walls as revealed in Fig. 1. The walls of

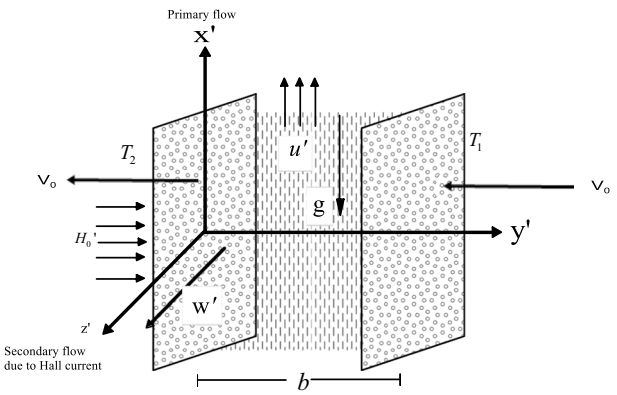


**Fig. 1** Flow description

the microchannel are subjected to surrounding temperatures: $T_1$ at the right wall and $T_2$ at the left wall and assuming $T_1 > T_2$. Also, the magnitude of Reynolds number is assumed to be almost insignificant such that the magnetic induction effects could be neglected. It is anticipated that a constant suction/injection velocity $\left(v_0'\right)$ is supplied to the porous walls. Initially, the hydromagnetic and thermal flow is taken along the vertical $x'$-axis; however, as a result of the influence of Hall current, secondary flow (induced flow) is generated along the $z'$-direction. Hence, the velocity field and magnetic field are of the form: $\vec{V} = \left(u', v_0', w'\right)$ and $\vec{B} = \left(0, H_0', 0\right)$.

The generalized Ohm's law in the existence of Hall current and ion-slip effect is of the form (Sutton and Sherman [32]):

$$\vec{J} = \sigma\left[\vec{E} + \left(\vec{V} \times \vec{B}\right)\right] - \frac{\beta_{\mathrm{h}}}{H_0}\left(\vec{J} \times \vec{B}\right) + \frac{\beta_{\mathrm{h}}\beta_{\mathrm{i}}}{H_0^2}\left(\vec{J} \times \vec{B}\right) \times \vec{B}. \tag{1}$$

Following Jha et al. [31], and combining the influence of ion-slip currents, the flow equations under the Boussinesq approximation takes the form:

Momentum equations along primary flow direction:

$$\upsilon_{\mathrm{r}}\frac{\mathrm{d}^2u'}{\mathrm{d}y'^2} - v_0'\frac{\mathrm{d}u'}{\mathrm{d}y'} + g\beta_{\mathrm{r}}(T - T_{\mathrm{r}}) - \frac{\sigma_{\mathrm{r}}\mu_e^2H_0^2}{(\alpha_e^2 + \beta_{\mathrm{h}}^2)\rho_{\mathrm{r}}}(\alpha_e u' + \beta_{\mathrm{h}}w') = 0, \tag{2}$$

Momentum equations along secondary (induced flow) direction:

$$\upsilon_{\mathrm{r}}\frac{\mathrm{d}^2w'}{\mathrm{d}y'^2} - v_0'\frac{\mathrm{d}w'}{\mathrm{d}y'} + \frac{\sigma_{\mathrm{r}}\mu_e^2H_0^2}{(\alpha_e^2 + \beta_{\mathrm{h}}^2)\rho_{\mathrm{r}}}(\beta_{\mathrm{h}}u' - \alpha_e w') = 0, \tag{3}$$

Energy equation:

$$\alpha_{\mathrm{r}}\frac{\mathrm{d}^2T'}{\mathrm{d}y'^2} - v_0'\frac{\mathrm{d}T'}{\mathrm{d}y'} = 0. \tag{4}$$

With boundary situations:

$$u' = \frac{2 - f_v}{f_v}\lambda_r\frac{\mathrm{d}u'}{\mathrm{d}y'}\Big|_{y'=0}, \quad w' = \frac{2 - f_v}{f_v}\lambda_r\frac{\mathrm{d}w'}{\mathrm{d}y'}\Big|_{y'=0}, \quad T' = T_2 + \frac{2 - f_t}{f_t}\frac{2\gamma_{\mathrm{s}}}{\gamma_{\mathrm{s}} + 1}\frac{\lambda_{\mathrm{r}}}{\mathrm{Pr}}\frac{\mathrm{d}T'}{\mathrm{d}y'}\Big|_{y'=0}, \tag{5}$$

$$u' = -\frac{2 - f_v}{f_v}\lambda_{\mathrm{r}}\frac{\mathrm{d}u'}{\mathrm{d}y'}\Big|_{y'=b}, \quad w' = -\frac{2 - f_v}{f_v}\lambda_{\mathrm{r}}\frac{\mathrm{d}w'}{\mathrm{d}y'}\Big|_{y'=b}, \quad T' = T_1 - \frac{2 - f_t}{f_t}\frac{2\gamma_{\mathrm{s}}}{\gamma_{\mathrm{s}} + 1}\frac{\lambda_r}{\mathrm{Pr}}\frac{\mathrm{d}T'}{\mathrm{d}y'}\Big|_{y'=b}, \tag{6}$$

By engaging the quantities:

$$\begin{aligned} &y = \frac{y'}{b}, \quad M^2 = \frac{\sigma_{\mathrm{r}}\mu_e^2H_0^2b^2}{\mu_{\mathrm{r}}}, \quad (u, w) = \frac{(u', w')}{U_c}, \quad U_c = \frac{\rho_{\mathrm{r}}g\beta_{\mathrm{r}}(T_1 - T_{\mathrm{r}})b^2}{\mu_{\mathrm{r}}}, \\ &\theta = \frac{T' - T_{\mathrm{r}}}{T_1 - T_{\mathrm{r}}}, \quad S = \frac{v_0'b}{\upsilon_r}, \quad \mathrm{Pr} = \frac{\upsilon_{\mathrm{r}}}{\alpha_{\mathrm{r}}}, \upsilon_{\mathrm{r}} = \frac{\mu_{\mathrm{r}}}{\rho_{\mathrm{r}}}. \end{aligned} \tag{7}$$

Following Jha et al. [31], Eqs. (2)–(4) subject to boundary conditions (5), (6) can be rewritten as:

$$\frac{\mathrm{d}^2u}{\mathrm{d}y^2} - S\frac{\mathrm{d}u}{\mathrm{d}y} + \theta - M^2\frac{(\alpha_e u + \beta_\mathrm{h} w)}{(\alpha_e^2 + \beta_\mathrm{h}^2)} = 0, \tag{8}$$

$$\frac{\mathrm{d}^2w}{\mathrm{d}y^2} - S\frac{\mathrm{d}w}{\mathrm{d}y} + M^2\frac{(\beta_\mathrm{h} u - \alpha_e w)}{(\alpha_e^2 + \beta_\mathrm{h}^2)} = 0, \tag{9}$$

$$\frac{\mathrm{d}^2\theta}{\mathrm{d}y^2} - S\,\mathrm{Pr}\,\frac{\mathrm{d}\theta}{\mathrm{d}y} = 0, \tag{10}$$

With dimensionless momentum and thermal boundary situations:

$$u(y) = \beta_\mathrm{v}\mathrm{Kn}\frac{\mathrm{d}u}{\mathrm{d}y}\Big|_{y=0}, \quad w(y) = \beta_\mathrm{v}\mathrm{Kn}\frac{\mathrm{d}w}{\mathrm{d}y}\Big|_{y=0}, \quad \theta(y) = \xi + \beta_\mathrm{v}\mathrm{Kn}\,\mathrm{In}\,\frac{\mathrm{d}\theta}{\mathrm{d}y}\Big|_{y=0}, \tag{11}$$

$$u(y) = -\beta_\mathrm{v}\mathrm{Kn}\frac{\mathrm{d}u}{\mathrm{d}y}\Big|_{y=1}, \quad w(y) = -\beta_\mathrm{v}\mathrm{Kn}\frac{\mathrm{d}w}{\mathrm{d}y}\Big|_{y=1}, \quad \theta(y) = 1 - \beta_\mathrm{v}\mathrm{Kn}\,\mathrm{In}\,\frac{\mathrm{d}\theta}{\mathrm{d}y}\Big|_{y=1} \tag{12}$$

It is interesting to note that since the hydromagnetic flow is regarded at the microscale level, fluid flow neighboring to the surfaces is not in thermal equilibrium. As a result, the fluid no longer reaches the velocity or temperature of the wall surface, necessitating the use of a slip condition for the velocity and a jump condition for the temperature. The usual continuum approach is used in this analysis by the continuum equations with the two main characteristics involved in microscale flow phenomena: velocity slip and temperature jump. In the present work, the boundary condition incorporating the velocity slip and temperature jump situations is defined following Jha and Malgwi [22] as:

$$u_s = -\frac{2-f_\mathrm{v}}{f_\mathrm{v}}\lambda\frac{\partial u}{\partial z}|_{z=b}, \text{and } T_\mathrm{s} - T_w = -\frac{2-f_\mathrm{t}}{f_\mathrm{t}}\frac{2\gamma}{\gamma+1}\frac{\lambda}{\mathrm{Pr}}\frac{\partial T}{\partial z}|_{z=b}, \tag{13}$$

where

$$\beta_\mathrm{v} = \frac{2-f_\mathrm{v}}{f_\mathrm{v}}, \quad \beta_\mathrm{t} = \frac{2-f_\mathrm{t}}{f_\mathrm{t}}\frac{2\gamma_\mathrm{s}}{\gamma_\mathrm{s}+1}\frac{1}{\mathrm{Pr}}, \quad \mathrm{Kn} = \frac{\lambda_\mathrm{r}}{b}, \quad \mathrm{In} = \frac{\beta_\mathrm{t}}{\beta_\mathrm{v}}, \quad \xi = \frac{T_2 - T_\mathrm{r}}{T_1 - T_\mathrm{r}}, \text{and } \alpha_e = 1+\beta_\mathrm{h}\beta_\mathrm{i}.$$

Numerical values for Pr, $\lambda_\mathrm{r}$, $\gamma_\mathrm{s}$ $f_\mathrm{v}$ and $f_\mathrm{t}$ are adopted following Eckert and Drake [33].
Assuming $F = u + iw$, Eqs. (8) and (9) simplify to:

$$\frac{\mathrm{d}^2F}{\mathrm{d}y^2} - S\frac{\mathrm{d}F}{\mathrm{d}y} + \theta - M_1^2F = 0, \tag{14}$$

with $M_1^2 = \frac{M^2}{\alpha_e + i\beta_\mathrm{h}}$.
Similarly, boundary wall conditions in Eqs. (11) and (12) simplify to:

$$\theta(y) = \xi + \beta_\mathrm{v}\mathrm{Kn}\,\mathrm{In}\,\frac{\mathrm{d}\theta}{\mathrm{d}y}, \quad F(y) = \beta_\mathrm{v}\mathrm{Kn}\frac{\mathrm{d}F}{\mathrm{d}y}, \text{at } y = 0, \tag{15}$$

$$\theta(y) = 1 - \beta_{\mathrm{v}}\mathrm{Kn}\ln\frac{\mathrm{d}\theta}{\mathrm{d}y}, \quad F(y) = -\beta_{\mathrm{v}}\mathrm{Kn}\frac{\mathrm{d}F}{\mathrm{d}y}, \text{at } y = 1 \tag{16}$$

Hence, the solutions to Eqs. (13) and (10) can be rendered as:

$$\theta(y) = A + B\exp\left(S\,\mathrm{Pr}\,y\right), \tag{17}$$

$$F(y) = C_1\exp(K_1 y) + C_2\exp(K_2 y) + \frac{A}{M_1^2} - C\exp(S\,\mathrm{Pr}\,y). \tag{18}$$

where $A,\ B,\ C_1,\ C_2\,C,\ K_1$ and $K_2$ are clear in the Appendix.

Interesting flow features involved in microfluidic flow like volume flow rate ($Q$) and shear stress ($\tau$) are also rendered as:

$$Q = \int_0^1 F(y)\mathrm{d}y. \tag{19}$$

Substituting (18) into (19) becomes:

$$Q = \frac{C_1}{K_1}[\exp(K_1) - 1] + \frac{C_2}{K_2}[\exp(K_2) - 1] + \frac{A}{M_1^2} - \frac{K_3}{S\,\mathrm{Pr}}[\exp(S\,\mathrm{Pr}) - 1] \tag{20}$$

using $Q_x = \mathrm{Real}(Q)$ and $Q_z = \mathrm{Imag}(Q)$.

Likewise, the shear stress about the microporous channel along the main and induced flow directions is defined as follows:

$$\begin{aligned}\tau_{x0} + i\tau_{z0} &= \frac{\mathrm{d}F}{\mathrm{d}y}\Big|_{y=0} \\ &= C_1K_1 + C_2K_2 - K_3S\,\mathrm{Pr},\end{aligned} \tag{21}$$

$$\begin{aligned}\tau_{x1} + i\tau_{z1} &= \frac{\mathrm{d}F}{\mathrm{d}y}\Big|_{y=1} \\ &= C_1K_1e^{K_1} + C_2K_2e^{K_2} - K_3S\,\mathrm{Pr}\,e^{S\,\mathrm{Pr}},\end{aligned} \tag{22}$$

where $\tau_x = \mathrm{Real}\left(\frac{\mathrm{d}F}{\mathrm{d}y}\right)$ and $\tau_z = \mathrm{Imag}\left(\frac{\mathrm{d}F}{\mathrm{d}y}\right)$.

## Discussion

Throughout this section, analysis on the influence of Hall parameter and ion-slip current on steady hydromagnetic flow in the occurrence of magnetic field will be investigated. Using the exact solutions obtained in the previous section, a MATLAB code was prepared to illustrate some interesting flow behaviors using line graphs. During the course of the investigation, reasonable range of value for various flow parameters include: $0.0 \le \beta_{\mathrm{v}}\mathrm{Kn} \le 0.1$, $0.01 \le \beta_{\mathrm{h}} \le 0.10$, $1.0 \le \beta_{\mathrm{i}} \le 9.0$, $0.5 \le S \le 1.5$ and $2 \le M \le 4$ with fixed values $\beta_{\mathrm{v}}\mathrm{Kn} = 0.05, l = 1.667, S = 0.5, \beta_{\mathrm{h}} = 0.10, \alpha_e = 3.0,$ and $M = 2.0$. The novelty of the present work is that the influence of various governing parameters was investigated for three cases of the wall–ambient temperature difference ratio ($\xi$) in the occurrence of Hall effect ($\beta_{\mathrm{h}}$) and ion-slip current ($\beta_i$): $\xi = 1$ suggests that the two walls

are heated with equal temperatures (symmetric), $\xi = 0$ suggests only one of the walls is heated (asymmetric), and $\xi = -1$ suggests one of the walls is heated and the other wall is cooled (asymmetric).

The solution for energy equation as given in Eq. (16) is the same with that of Jha et al. [31] in the slip regime. Hence, active flow parameters on temperature distribution have been comprehensively considered in [31].

Furthermore, numerical solution and values for velocity in the absence of Hall current ($\beta_e$) and ion-slip parameter ($\beta_\mathrm{i}$) found in the existing work were compared with Jha et al. [31] and are presented in Table 1. From the results reported, an excellent agreement is found, thus validating the solution obtained.

Figure 2a, b displays the combined effect of wall–ambient temperature difference ratio ($\xi$) and rarefaction parameter ($\beta_\mathrm{v}\mathrm{Kn}$) on the main and induced fluid velocity distribution profiles in the occurrence of Hall and ion-slip current. From the figure, it is evident that for $\xi = 1$ and $\xi = 0$, both the main flow velocity and induced velocity increase with $\beta_\mathrm{v}\mathrm{Kn}$, while they decrease for asymmetric heating ($\xi = -1$). The impeding influence of the microporous walls diminishes with the rise in rarefaction parameter ($\beta_\mathrm{v}\mathrm{Kn}$), thereby boosting both components of the fluid velocity. In addition, it is interesting to observe that the effect of $\beta_\mathrm{v}\mathrm{Kn}$ on velocity becomes stronger and more pronounced in a situation where the surrounding microporous walls are heated equally ($\xi = 1$).

Figure 3a, b shows the combined effect of wall–ambient temperature difference ratio ($\xi$) and Hartmann number ($M$) on the main and induced velocity profiles. Figure 3a reveals the effect of Hartmann number ($M$) on the main fluid velocity in the occurrence of Hall and ion-slip. The figure shows that a rise in Hartmann number weakens velocity when the surrounding wall temperatures are equal ($\xi = 1$) and when only one of the surrounding wall is heated ($\xi = 0$). The contrast is revealed when $\xi = -1$. The justification of this on the hydrodynamics is due to a rise in mechanical resistive force with an increase in Hartmann number. The reverse of this behavior is shown in Fig. 3b.

Figures 4 and 5 illuminate the impact suction/injection on the main flow and induced components of velocity under different surrounding temperatures ($\xi$). From the figure,

**Table 1** Evaluation of velocity in the existing work (in the absence of Hall effect and ion-slip current) with Jha et al. [31] when $M = 2.0, P_m = 0.5, S = 0.5, \beta_\mathrm{v}\mathrm{Kn} = 0.05, \mathrm{In} = 1.667$

| $\xi$ | $y$ | **Jha et al. [31]** | **Present work (when $\beta_\mathrm{h} = 0.0, \beta_\mathrm{i} = 1.0$)** |
|---|---|---|---|
| 1 | 0.2 | 0.0809 | 0.0809 |
| | 0.4 | 0.1137 | 0.1137 |
| | 0.6 | 0.1171 | 0.1171 |
| | 0.8 | 0.0885 | 0.0885 |
| 0 | 0.2 | 0.0284 | 0.0284 |
| | 0.4 | 0.0470 | 0.0470 |
| | 0.6 | 0.0561 | 0.0561 |
| | 0.8 | 0.0483 | 0.0483 |
| − 1 | 0.2 | − 0.0241 | − 0.0241 |
| | 0.4 | − 0.0196 | − 0.0196 |
| | 0.6 | − 0.0049 | − 0.0049 |
| | 0.8 | 0.0080 | 0.0080 |

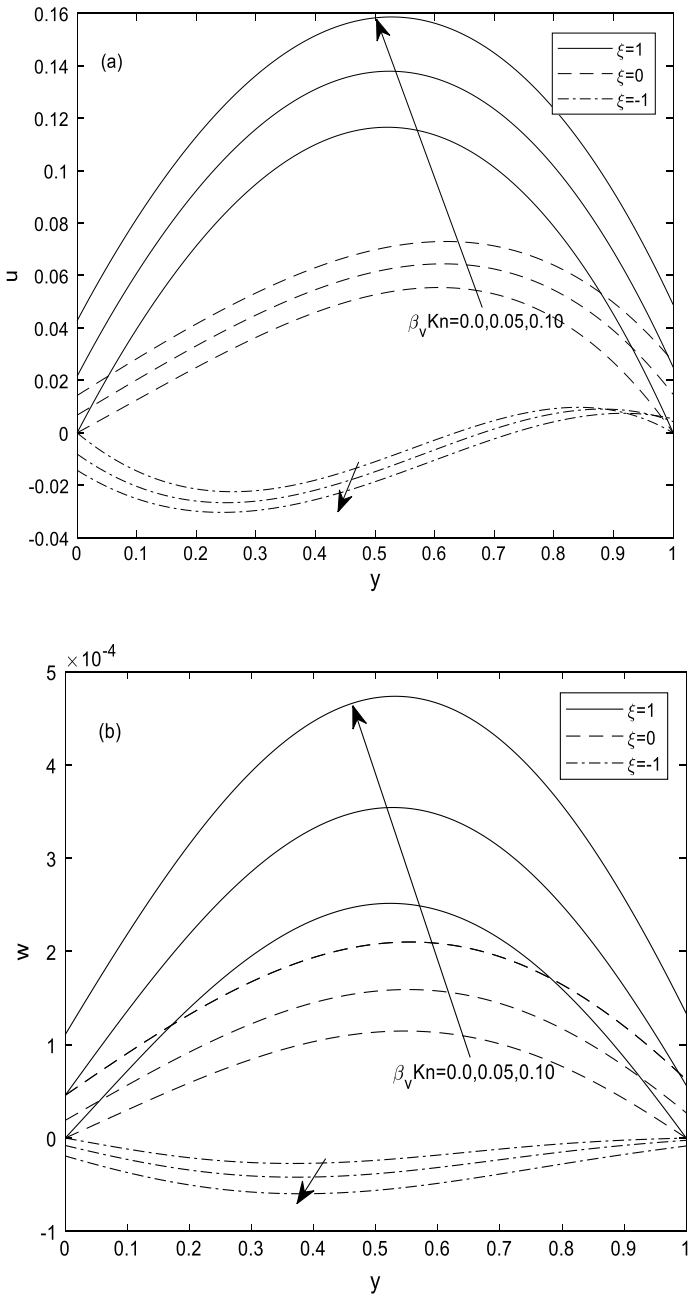


**Fig. 2** **a** Rarefaction parameter ($\beta_v$Kn) on the main flow and induced velocity profiles, for $M = 2, S = 0.5, \text{In} = 1.667, \beta_h = 0.10, \beta_i = 3.0$ and $\text{Pr} = 0.71$. **b** Rarefaction parameter ($\beta_v$Kn) on the main flow and induced velocity profiles, for $M = 2, S = 0.5, \text{In} = 1.667, \beta_h = 0.10, \beta_i = 3.0$ and $\text{Pr} = 0.71$

it is evident that both the main flow and induced components of fluid velocity decrease with injection for all considered values of $\xi$, while the reverse behavior is seen with suction (Fig. 5).

Figure 6 displays the effects of Hall current parameter ($\beta_h$) on the main flow and induced velocity within the microporous channel for different wall heating conditions ($\xi$). The figure reveals that in the occurrence of ion-slip, the main flow velocity

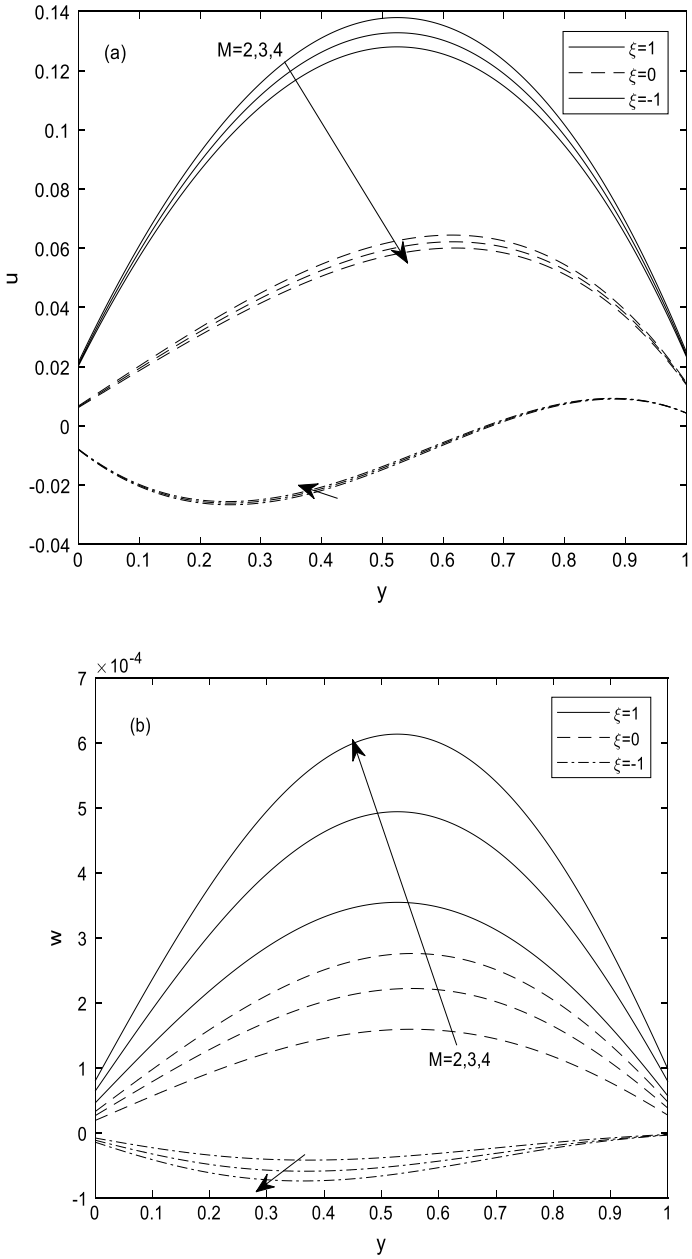


**Fig. 3** **a** Hartmann number ($M$) on the main flow and induced velocity profiles, for $\beta_v \mathrm{Kn} = 0.05, S = 0.5, \mathrm{In} = 1.667, \beta_h = 0.10, \beta_i = 3.0$ and $\mathrm{Pr} = 0.71$. **b** Hartmann number ($M$) on the main flow and induced velocity profiles, for $\beta_v \mathrm{Kn} = 0.05, S = 0.5, \mathrm{In} = 1.667, \beta_h = 0.10, \beta_i = 3.0$ and $\mathrm{Pr} = 0.71$

is insensitive to a rise in Hall parameter ($\beta_h$) for $\xi = 1$, $\xi = 0$ and $\xi = -1$ surrounding situations. When the induced flow component is considered on the other hand, it is worth noting that a rise in Hall parameter augments induced velocity distribution for $\xi = 1$ and $\xi = 0$ wall heating situations.

The effect of ion-slip current ($\beta_i$) on the main flow and induced fluid velocity profiles is depicted in Fig. 7a, b. Illustrations from the figure suggest that for $\xi = 1$ and $\xi = 0$ wall heating conditions, introducing ion-slip current ($\beta_i$) aids the flow along the main flow

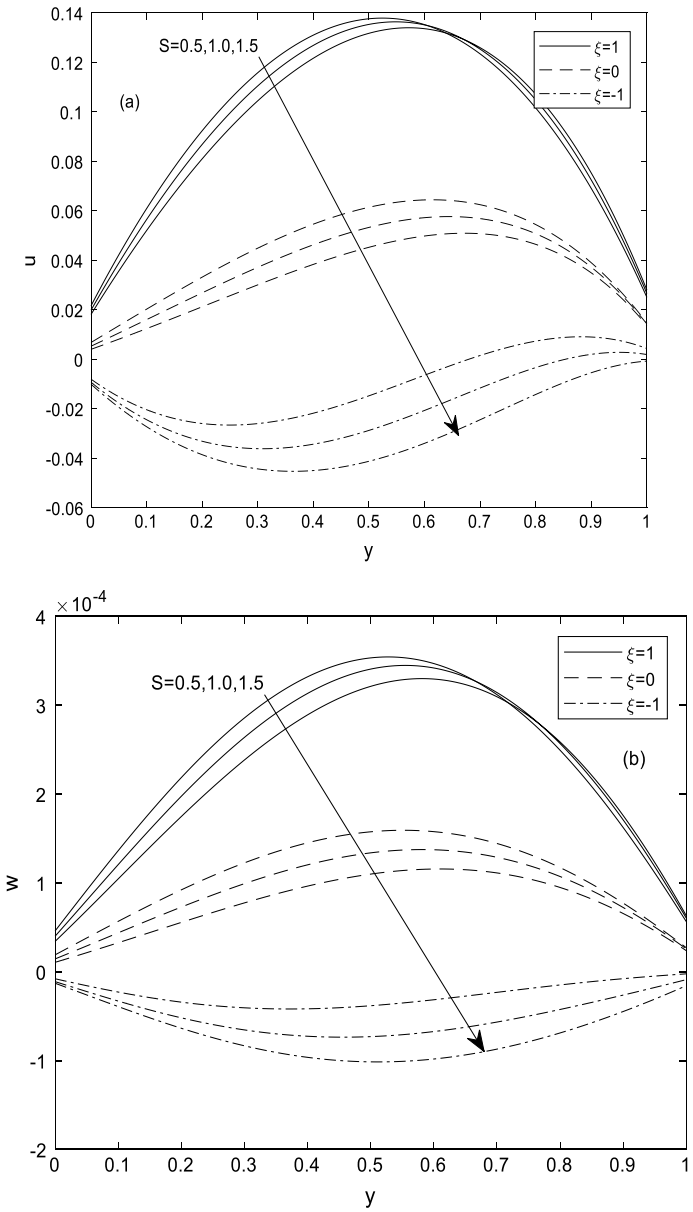


**Fig. 4** **a** Injection (positive value of $S$) on the main flow and induced velocity profiles, for $\beta_{\mathrm{v}}\mathrm{Kn} = 0.05, M = 2, \mathrm{In} = 1.667, \beta_{\mathrm{h}} = 0.10, \beta_{\mathrm{i}} = 3.0$ and $\mathrm{Pr} = 0.71$. **b** Injection (positive value of $S$) on the main flow and induced velocity profiles, for $\beta_{\mathrm{v}}\mathrm{Kn} = 0.05, M = 2, \mathrm{In} = 1.667, \beta_{\mathrm{h}} = 0.10, \alpha_e = 3.0$ and $\mathrm{Pr} = 0.71$

direction, causing a rise in velocity distribution, whereas it weakens the induced velocity. Also, the figure suggests that induced velocity weakens with a rise in $\beta_{\mathrm{i}}$ until the net velocity becomes zero. With the inclusion of Hall current, a rise in ion slip supports the magnetic lines of force, yielding a reduction in velocity profile.

Figures 8, 9, 10, 11, 12 and 13 demonstrate the variations of skin friction along the main flow and induced flow directions ($\tau_x, \tau_z$) with active flow parameters at $y = 0$ and $y = 1$ correspondingly. The combined effect of Hartmann number ($M$), rarefaction parameter ($\beta_{\mathrm{v}}\mathrm{Kn}$) and wall–ambient temperature difference ratio ($\xi$) on $\tau_{x0}$ and $\tau_{z0}$ is illustrated in

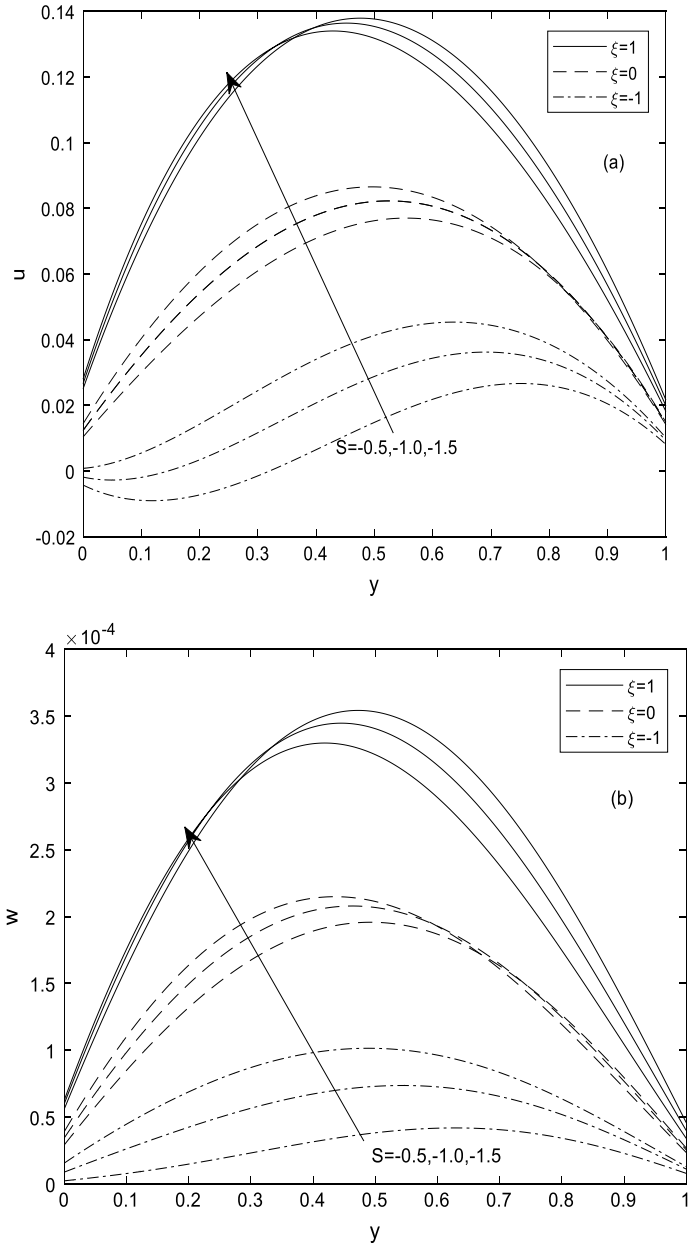


**Fig. 5** **a** Suction (negative value of *S*) on the main flow and induced velocity profiles, for $\beta_v \mathrm{Kn} = 0.05, M = 2, \mathrm{In} = 1.667, \beta_h = 0.10, \beta_i = 3.0$ and $\mathrm{Pr} = 0.71$. **b** Suction (negative value of *S*) on the main flow and induced velocity profiles, for $\beta_v \mathrm{Kn} = 0.05, M = 2, \mathrm{In} = 1.667, \beta_h = 0.10, \beta_i = 3.0$ and $\mathrm{Pr} = 0.71$

Fig. 8a, b at the wall $y = 0$. The figure shows that simultaneously growing $M$ and $\beta_v \mathrm{Kn}$ drops $\tau_{x0}$, while it rises $\tau_{z0}$ for $\xi = 1$ and $\xi = 0$ wall heating situations. From Fig. 9, on the other hand, it is observed that $\tau_{x1}$ decreases with $\beta_v \mathrm{Kn}$, whereas it increases with $M$. The contrast result is true and can be observed for $\tau_{z1}$ in Fig. 9b.

Figures 10 and 11 reveal that skin friction profile along the main flow direction at $y = 0$ and $y = 1$ identified as $\tau_{x0}$ and $\tau_{x1}$ remains insensitive to a rise in Hall parameter ($\beta_h$). However, a rise in wall–ambient temperature difference ratio ($\xi$) yields an increase in $\tau_{x0}$ and $\tau_{x1}$, respectively. On the other hand, the induced component of

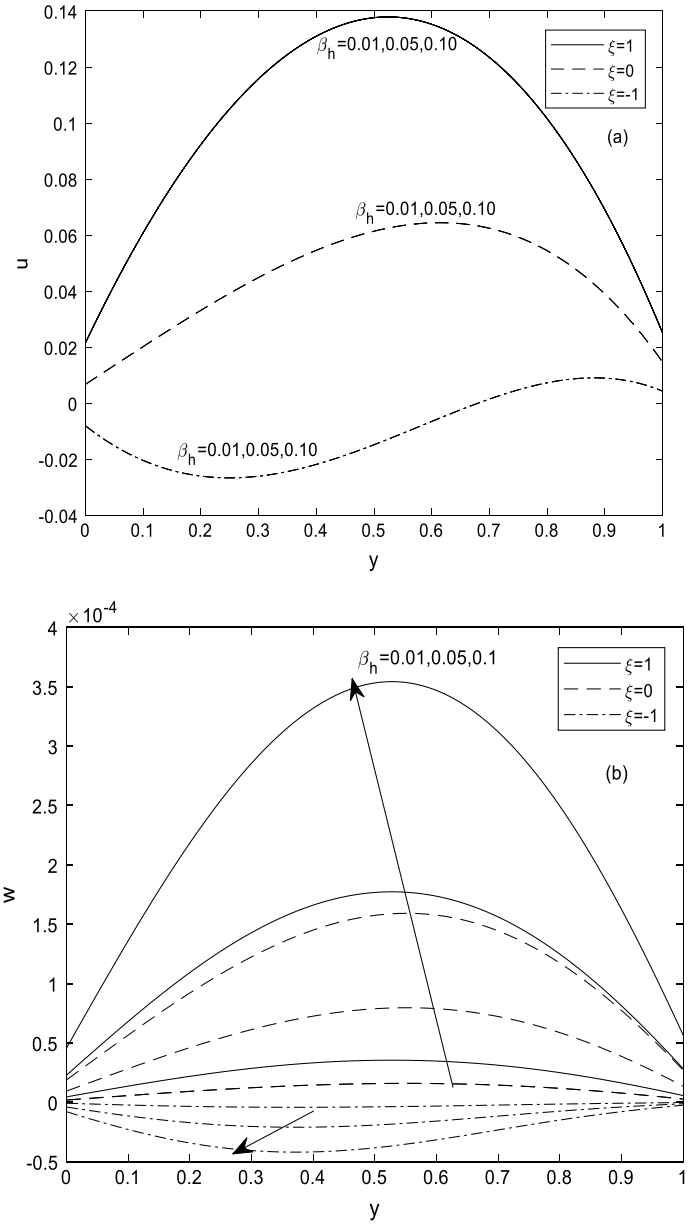


**Fig. 6** **a** Hall parameter ($\beta_h$) on the main flow and induced velocity profiles, for $\beta_v \mathrm{Kn} = 0.05, M = 2, \ln = 1.667, S = 0.5, \beta_i = 3.0$ and $\mathrm{Pr} = 0.71$. **b** Hall parameter ($\beta_h$) on the main flow and induced velocity profiles, for $\beta_v \mathrm{Kn} = 0.05, M = 2, \ln = 1.667, S = 0.5, \beta_i = 3.0$ and $\mathrm{Pr} = 0.71$

skin friction $\tau_{z0}$ and $\tau_{z1}$ is observed to increase with $\beta_h$ for $\xi = 1$ and $\xi = 0$ wall heating situations, whereas it decreases for $\xi = -1$.

The response of skin friction at the microchannel walls ($\tau_x$ and $\tau_z$) with variations in ion-slip current ($\beta_i$) and rarefaction parameter ($\beta_v \mathrm{Kn}$) is displayed in Figs. 12 and 13 for different values of $\xi$. From Fig. 12, it is observed that when either of the surrounding wall temperatures is the same or otherwise (symmetric/asymmetric:$\xi = 1$, $\xi = 0$), the skin friction ($\tau_{x0}$) along the main flow direction increases with ion-slip current irrespective of the value of the rarefaction parameter ($\beta_v \mathrm{Kn}$), whereas

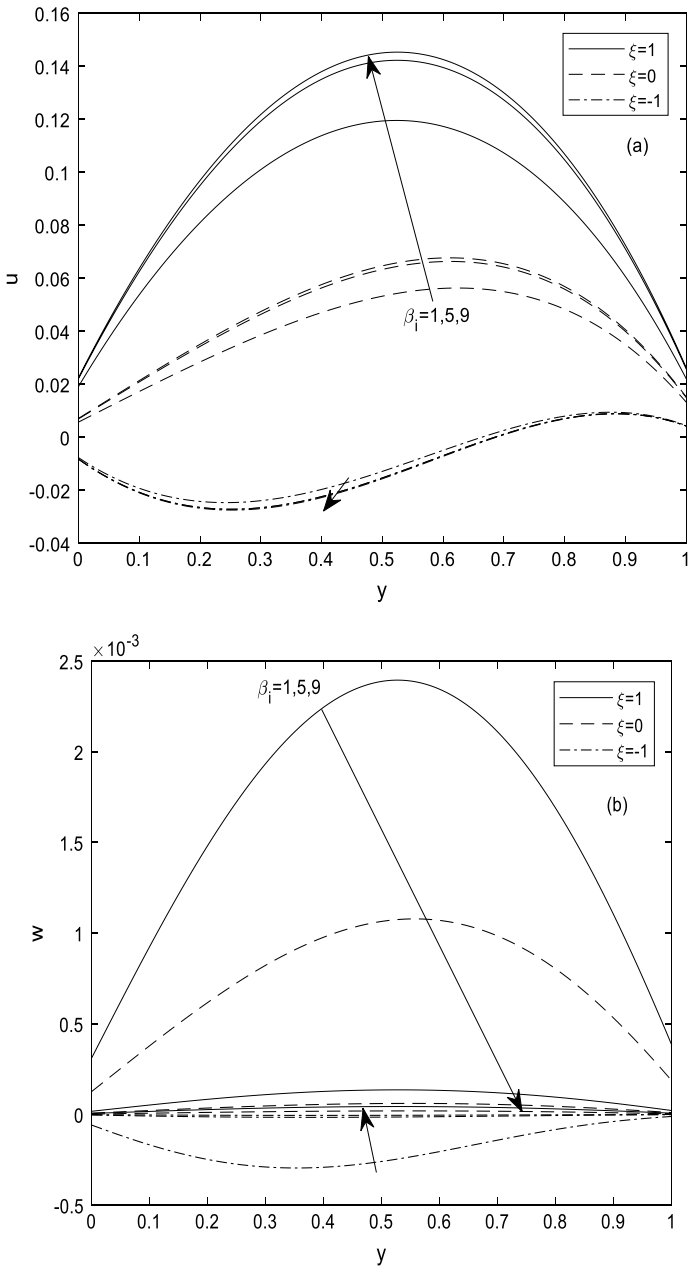


**Fig. 7** **a** Ion-slip parameter ($\beta_i$) on the main flow and induced velocity profiles, for $\beta_v \mathrm{Kn} = 0.05, M = 2, \ln = 1.667, S = 0.5, \beta_h = 0.10$ and $\mathrm{Pr} = 0.71$. **b** Ion-slip parameter ($\beta_i$) on the main flow and induced velocity profiles, for $\beta_v \mathrm{Kn} = 0.05, M = 2, \ln = 1.667, S = 0.5, \beta_h = 0.10$ and $\mathrm{Pr} = 0.71$

it decreases along the induced direction ($\tau_{z0}$). The reverse of this occurrence is shown in Fig. 13a, b at wall $y = 1$.

Figures 14, 15, 16 and 17 demonstrate the variations of the main flow and induced flow volume flow rate ($Q_x, Q_z$) with various flow parameters. The effect of injection (positive value of $S$) as well as wall–ambient temperature difference ratio ($\xi$) on volume flow rate alongside the main flow and induced flow direction, respectively, is depicted in Fig. 14a, b in the existence of Hall parameter ($\beta_h$) and ion-slip current

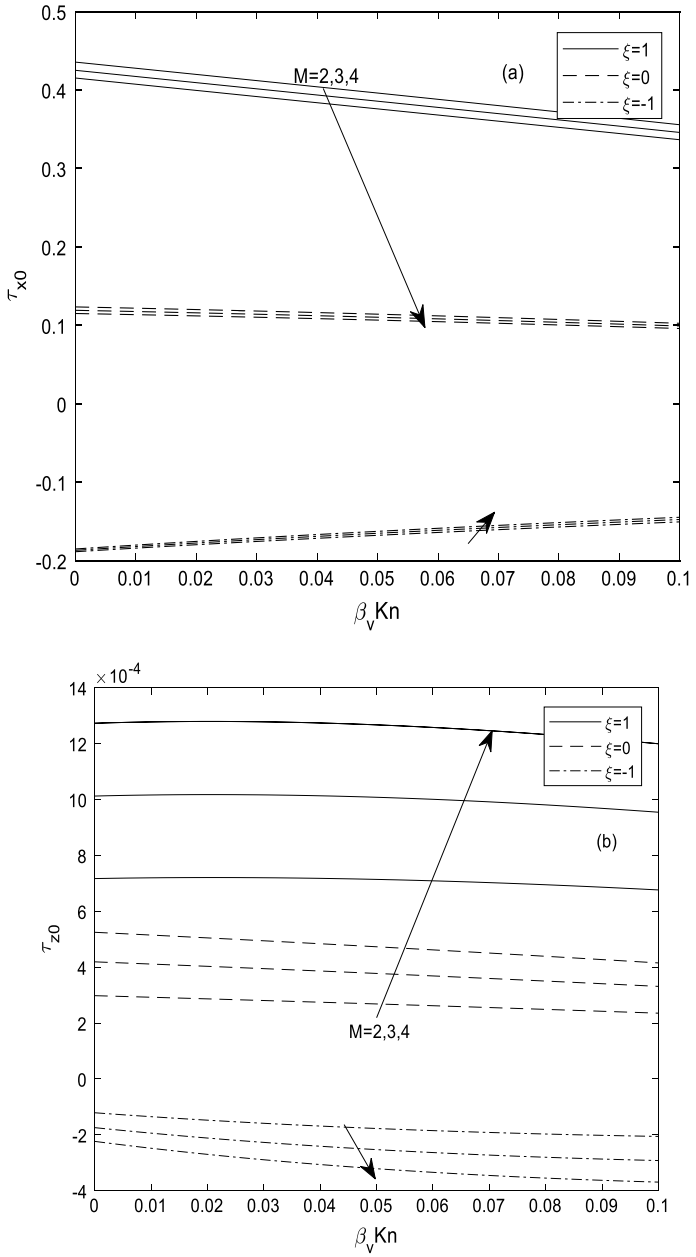


**Fig. 8** **a** Hartmann number ($M$) on the main flow and induced skin friction profiles at $y = 0$, for $S = 0.5$, ln $= 1.667$, $\beta_h = 0.5$, $\beta_i = 3.0$ and Pr $= 0.71$. **b** Hartmann number ($M$) on the main flow and induced skin friction profiles at $y = 0$, for $S = 0.5$, ln $= 1.667$, $\beta_h = 0.5$, $\beta_i = 3.0$ and Pr $= 0.71$

($\beta_i$). The figure shows that in a situation where $\xi = 1$, 0 or $-1$, an increase in injection yields a decline in both the main and induced volume flow rate profiles ($Q_x$, $Q_z$). In this case, the cold fluid particles are injected alongside the left cooler wall and sucked alongside the right heated wall, thereby horizontally reducing the convection current and consequently the volume flow. The reverse phenomenon is observed with suction as displayed in Fig. 15a, b. However, it is noted that suction enhances the volume flow for symmetric wall heating.

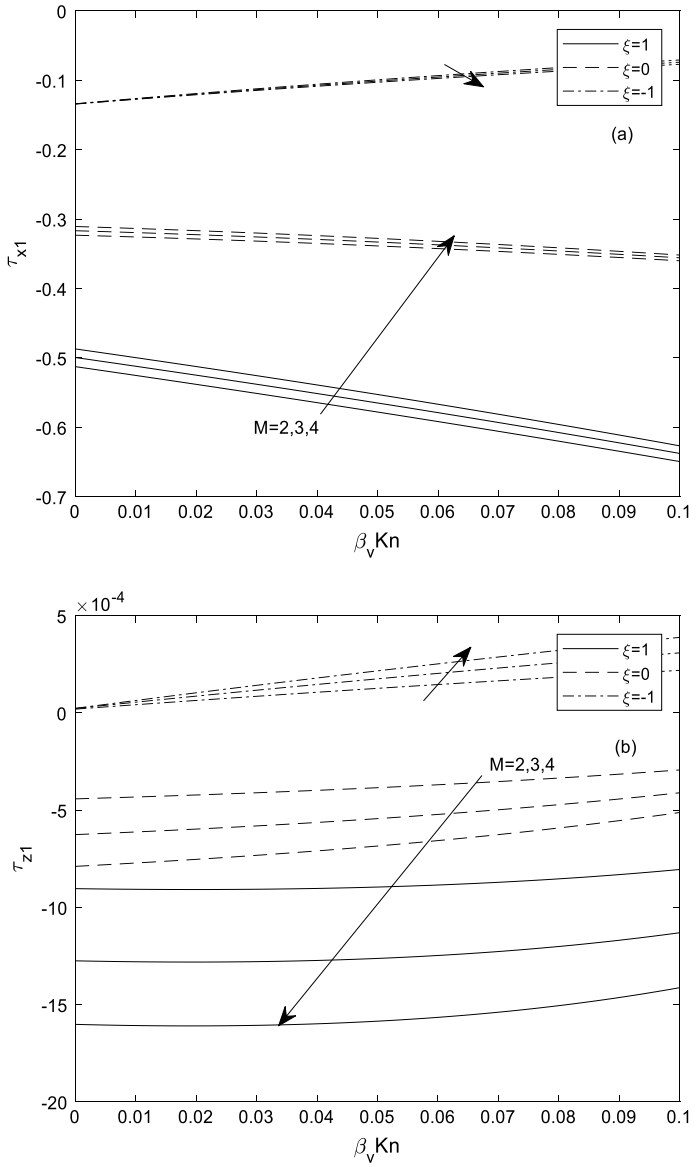


**Fig. 9** **a** Hartmann number ($M$) on the main flow and induced skin friction profiles at $y = 1$, for $\beta_v\text{Kn} = 0.05, M = 2, \text{In} = 1.667, \beta_h = 0.5, \beta_i = 3.0$ and $\text{Pr} = 0.71$. **b** Hartmann number ($M$) on the main flow and induced skin friction profiles at $y = 1$, for $\beta_v\text{Kn} = 0.05, M = 2, \text{In} = 1.667, \beta_h = 0.5, \beta_i = 3.0$ and $\text{Pr} = 0.71$

Figure 16 illustrates the effect of Hall current parameter ($\beta_h$) on volume flow rate distribution in the presence of suction/injection parameter ($S$) and ion-slip current ($\beta_i$). The results reveal that when the ion-slip current ($\beta_i$) is large and dominates the flow, the impact of Hall current becomes irrelevant on the main component of volume flow rate ($Q_x$) in the existence of rarefaction parameter ($\beta_v$Kn). When the induced component is considered on the other hand (Fig. 16b), it is evident that the effect of Hall parameter ($\beta_h$) on volume flow rate becomes more pronounced in the presence of wall–ambient temperature difference ratio ($\xi$). The figure suggests that an increase in $\beta_h$ causes an enhancement in $Q_z$ for $\xi = 1$ and $\xi = -1$, whereas it decreases for

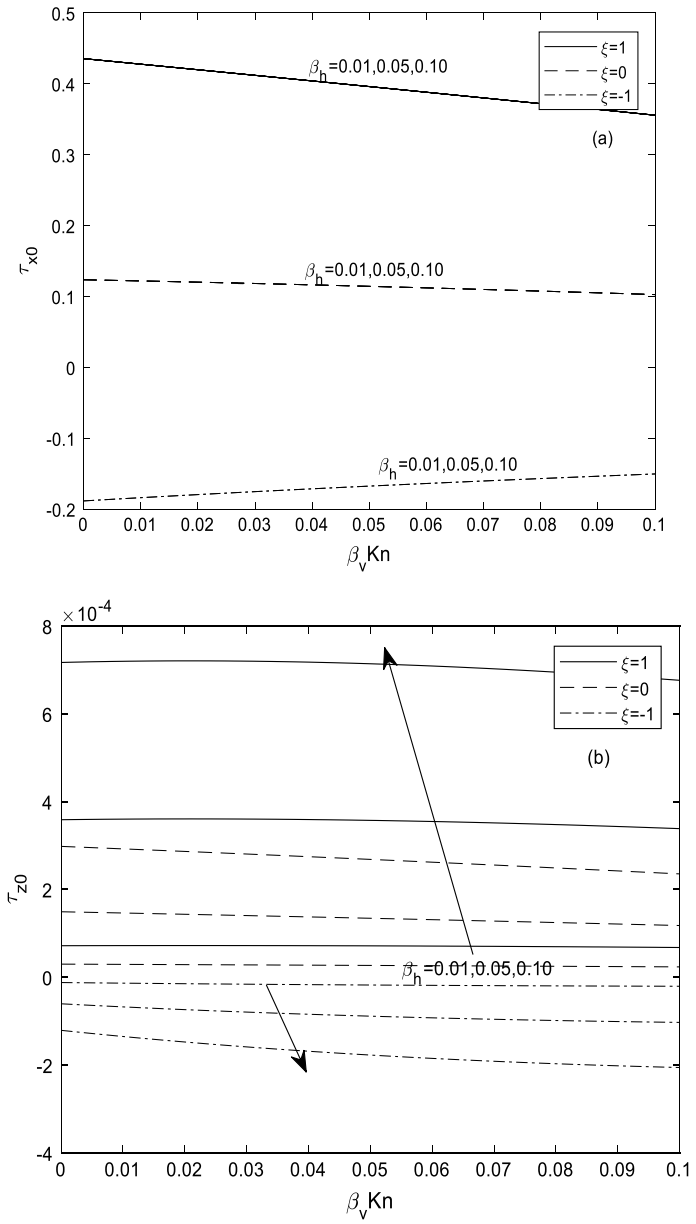


**Fig. 10** **a** Hall current ($\beta_h$) on the main flow and induced skin friction profiles at $y = 0$, for $\beta_v\text{Kn} = 0.05, M = 2, \text{In} = 1.667, M = 2.0, \beta_i = 3.0$ and $\text{Pr} = 0.71$. **b** Hall current ($\beta_h$) on the main flow and induced skin friction profiles at $y = 0$, for $\beta_v\text{Kn} = 0.05, M = 2, \text{In} = 1.667, M = 2.0, \beta_i = 3.0$ and $\text{Pr} = 0.71$

$\xi = 0$. The figure also suggests that $Q_z$ is unaffected with an increase in $\beta_v\text{Kn}$ for all considered values of $\beta_h$ and $\xi$.

From Fig. 17a, b, it is interesting to observe that ion-slip current ($\beta_i$) supports flow development alongside the vertical main flow direction, thereby augmenting the volume flow rate ($Q_x$) toward the main flow direction for $\xi = 1$ and $\xi = 0$, while a reverse flow is encountered for asymmetric heating ($\xi = -1$). The induced component of volume flow reveals a contrast of this behavior as an increase in ion-slip current destabilizes flow formation, causing the net volume flow to be zero for all wall heating situations.

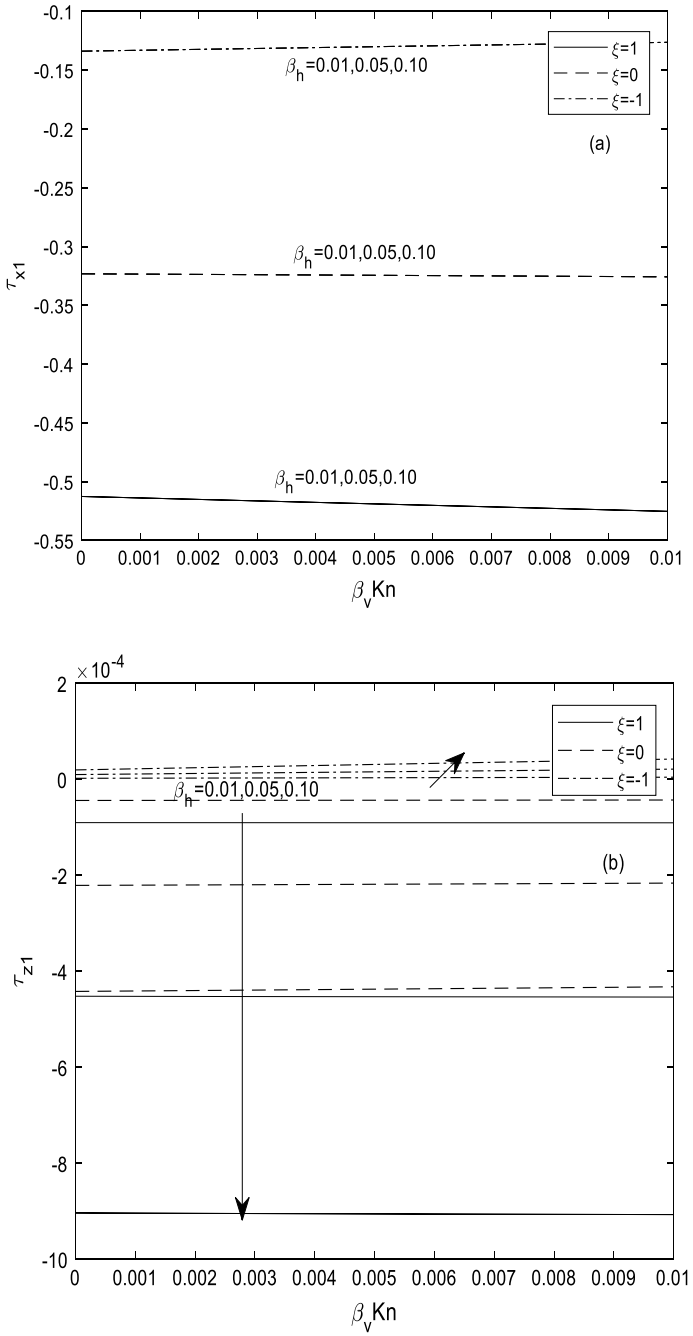


**Fig. 11** **a** Hall current ($\beta_h$) on the main flow and induced skin friction profiles at $y = 1$, for $\beta_v \mathrm{Kn} = 0.05, M = 2, \mathrm{ln} = 1.667, M = 2.0, \beta_i = 3.0$ and $\mathrm{Pr} = 0.71$. **b** Hall current ($\beta_h$) on the main flow and induced skin friction profiles at $y = 1$, for $\beta_v \mathrm{Kn} = 0.05, M = 2, \mathrm{ln} = 1.667, M = 2.0, \beta_i = 3.0$ and $\mathrm{Pr} = 0.71$

## Conclusion

In the present work, theoretical analysis on the combined effects of Hall current and ion-slip effects on magnetohydrodynamic flow is examined. Solutions to the flow equations are obtained analytically for fluid temperature, velocity, induced magnetic field, induced current density, volume flow rate and skin friction and are presented in

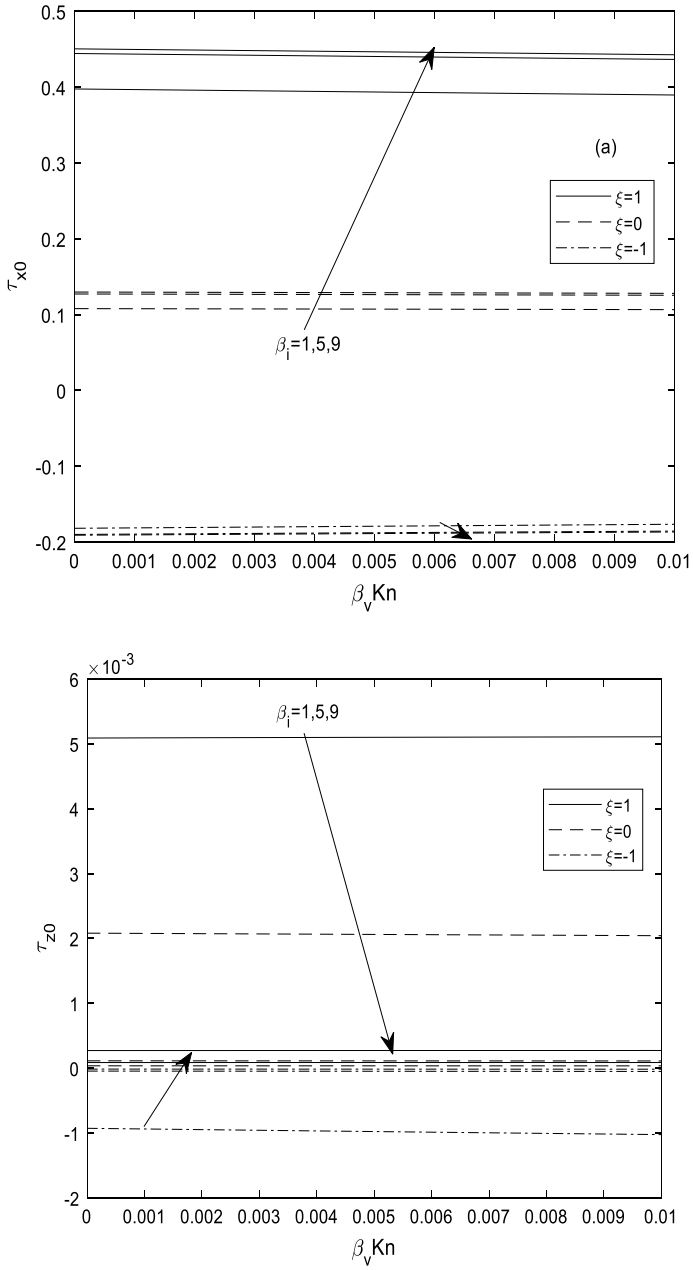


**Fig. 12** **a** Ion-slip parameter ($\beta_i$) on the main flow and induced skin friction profiles at $y = 0$, for $\beta_v \mathrm{Kn} = 0.05, M = 2, \mathrm{In} = 1.667, M = 2.0, \beta_h = 0.10$ and $\mathrm{Pr} = 0.71$. **b** Ion-slip parameter ($\beta_i$) on the main flow and induced skin friction profiles at $y = 0$, for $\beta_v \mathrm{Kn} = 0.05, M = 2, \mathrm{In} = 1.667, M = 2.0, \beta_h = 0.10$ and $\mathrm{Pr} = 0.71$

dimensionless form under relevant boundary conditions. The main conclusion of the analysis is that:

1. A rise in Hartmann number declines velocity distribution along the vertical main flow direction for symmetric ($\xi = 1$) and asymmetric wall heating ($\xi = 0$), whereas it increases along the induced flow direction.

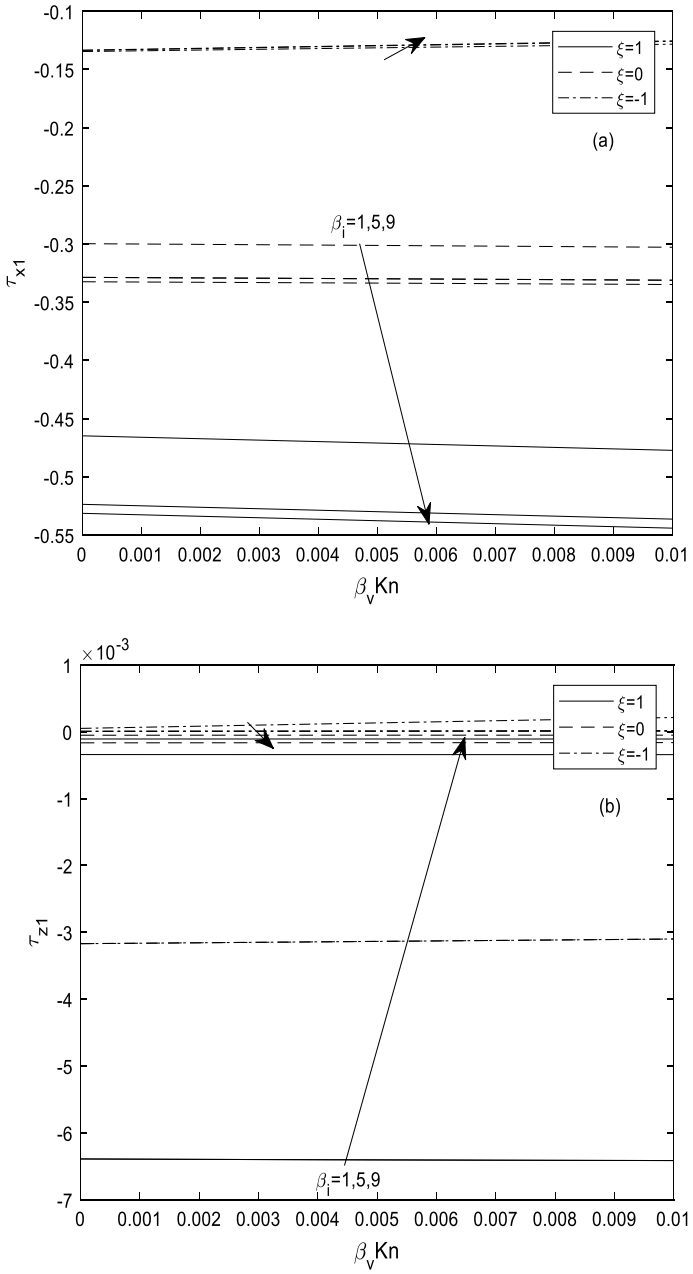


**Fig. 13** **a** Ion-slip parameter ($\beta_i$) on the main flow and induced skin friction profiles at $y = 1$, for $\beta_v\text{Kn} = 0.05, M = 2, \text{In} = 1.667, M = 2.0, \beta_h = 0.10$ and $\text{Pr} = 0.71$. **b** Ion-slip parameter ($\beta_i$) on the main flow and induced skin friction profiles at $y = 1$, for $\beta_v\text{Kn} = 0.05, M = 2, \text{In} = 1.667, M = 2.0, \beta_h = 0.10$ and $\text{Pr} = 0.71$

2. An increase in rarefaction parameter ($\beta_v$Kn) enhances the gas velocity in both the main flow and induced flow directions.
3. In the occurrence of ion-slip current, vertical main flow velocity and volume flow rate remain unchanged with an increase in Hall current parameter, whereas they increase along the induced flow direction.

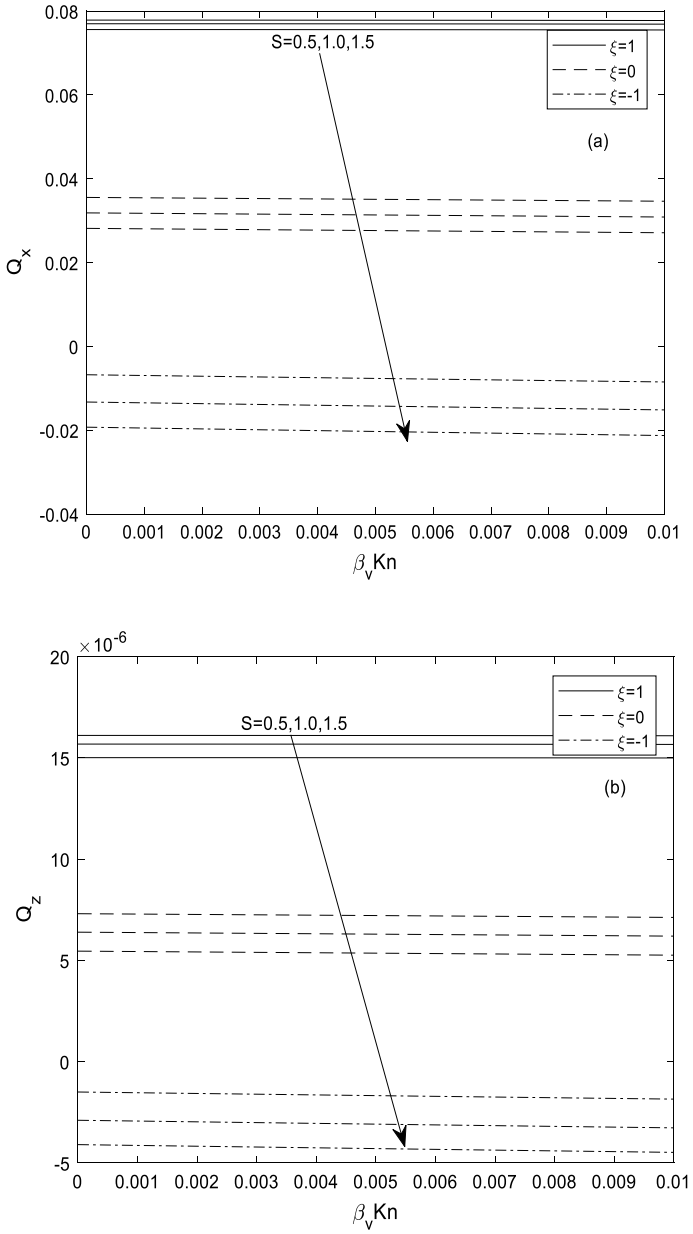


**Fig. 14** **a** Suction/injection parameter (positive value of *S*) on the main flow and induced volume flow rate for $\beta_v \mathrm{Kn} = 0.05, M = 2, \mathrm{In} = 1.667, \beta_i = 3.0, \beta_h = 0.10$ and $\mathrm{Pr} = 0.71$. **b** Suction/injection parameter (positive value of *S*) on the main flow and induced volume flow rate for $\beta_v \mathrm{Kn} = 0.05, M = 2, \mathrm{In} = 1.667, \beta_i = 3.0, \beta_h = 0.10$ and $\mathrm{Pr} = 0.71$

4. For all deliberated microchannel surrounding heating conditions ($\xi$) and rarefaction parameter ($\beta_v \mathrm{Kn}$), an increase in injection (positive value of S) declines both the main flow and induced volume flow rate.

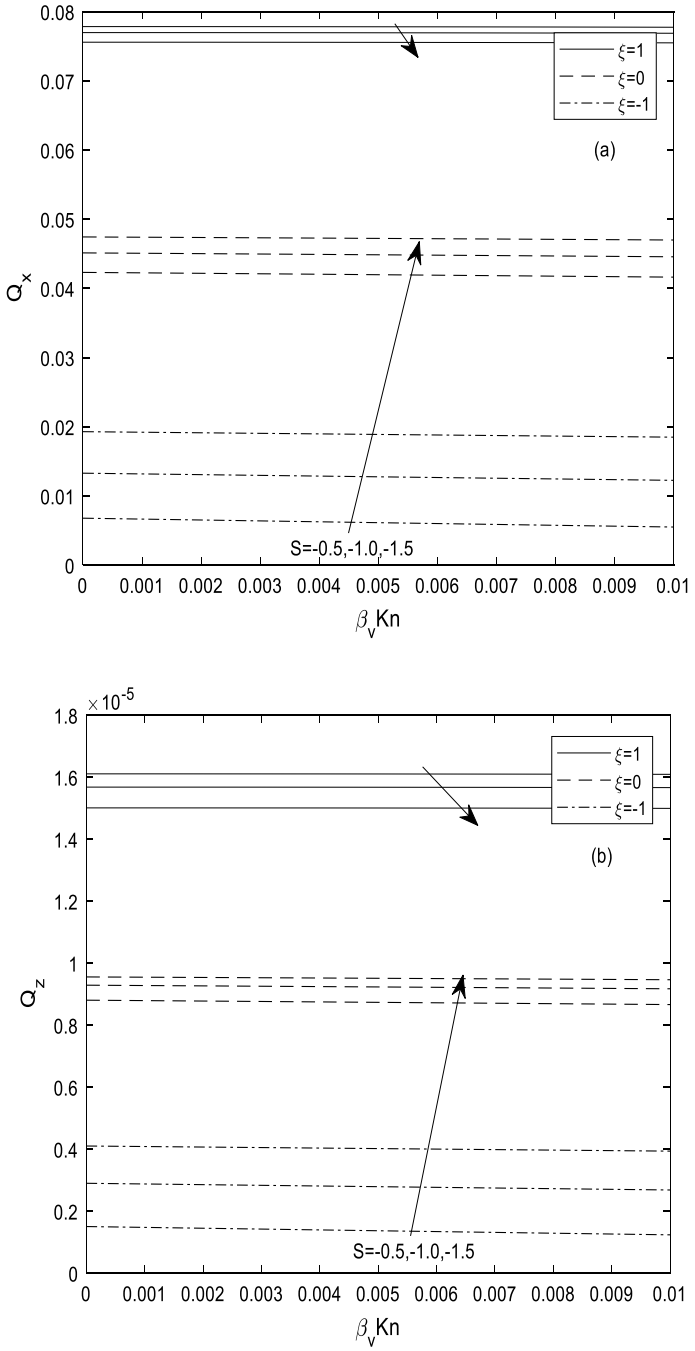


**Fig. 15** **a** Suction/injection parameter (negative value of $S$) on the main flow and induced volume flow rate for $\beta_v\mathrm{Kn} = 0.05, M = 2, \ln = 1.667, \beta_i = 3.0, \beta_h = 0.10$ and $\mathrm{Pr} = 0.71$. **b** Suction/injection parameter (negative value of $S$) on the main flow and induced volume flow rate for $\beta_v\mathrm{Kn} = 0.05, M = 2, \ln = 1.667, \beta_i = 3.0, \beta_h = 0.10$ and $\mathrm{Pr} = 0.71$

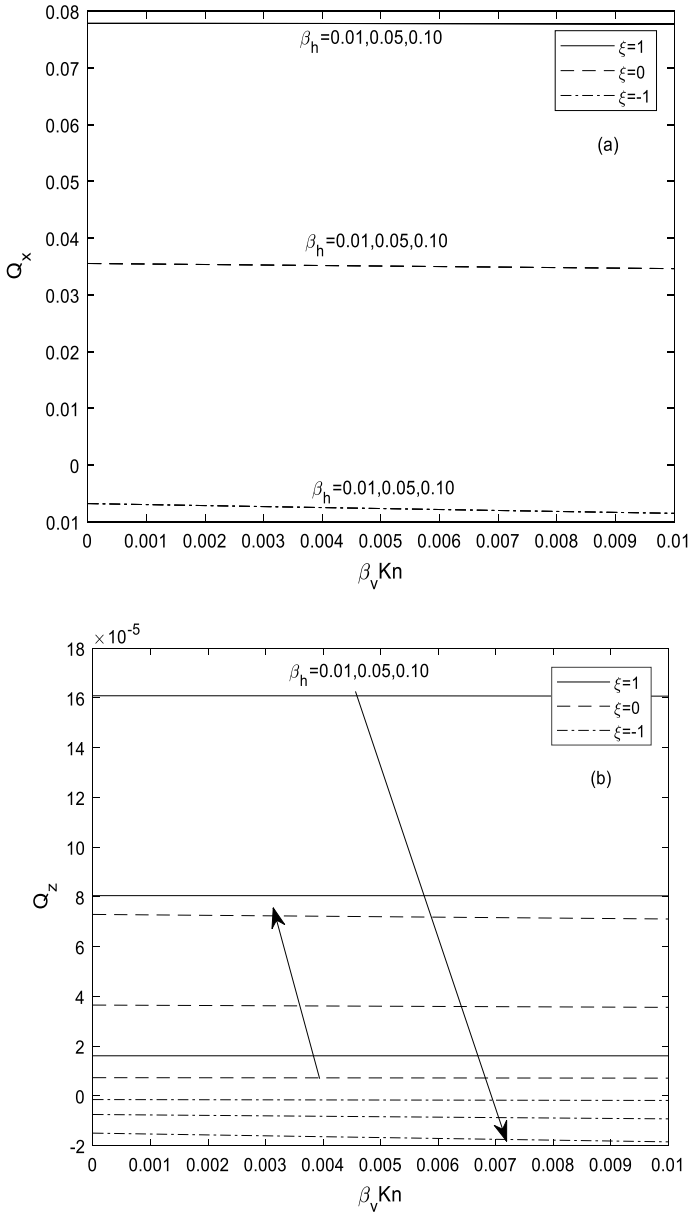


**Fig. 16** **a** Hall current parameter ($\beta_h$) on the main flow and induced volume flow rate for $\beta_v \mathrm{Kn} = 0.05, S = 0.5, M = 2, \mathrm{In} = 1.667, \beta_i = 3.0$ and $\mathrm{Pr} = 0.71$. **b** Hall current parameter ($\beta_h$) on the main flow and induced volume flow rate for $\beta_v \mathrm{Kn} = 0.05, S = 0.5, M = 2, \mathrm{In} = 1.667, \beta_i = 3.0$ and $\mathrm{Pr} = 0.71$

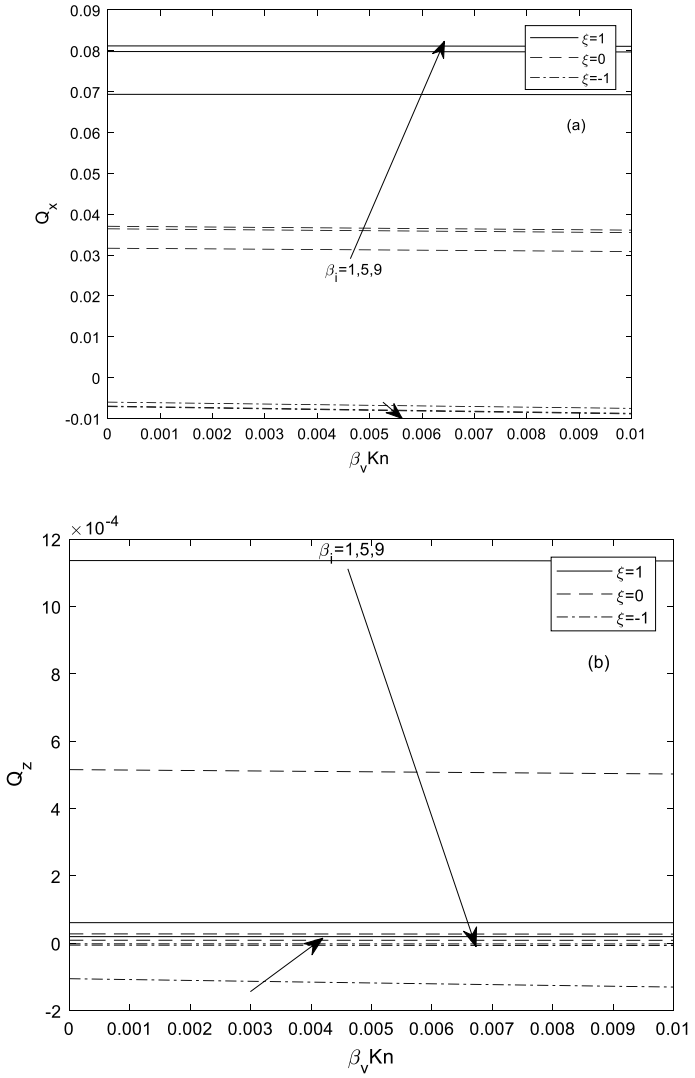


**Fig. 17** **a** Ion-slip current parameter ($\beta_i$) on the main flow and induced volume flow rate for $\beta_v \mathrm{Kn} = 0.05, S = 0.5, M = 2, \mathrm{In} = 1.667, \beta_h = 0.10$ and $\mathrm{Pr} = 0.71$. **b** Ion-slip current parameter ($\beta_i$) on the main flow and induced volume flow rate for $\beta_v \mathrm{Kn} = 0.05, S = 0.5, M = 2, \mathrm{In} = 1.667, \beta_h = 0.10$ and $\mathrm{Pr} = 0.71$

## Appendix

$$A_1 = 1 - \beta_v \mathrm{KnIn} S \,\mathrm{Pr}$$

$$A_2 = e^{S\,\mathrm{Pr}} + \beta_v \mathrm{KnIn} S \,\mathrm{Pr}\, e^{S\,\mathrm{Pr}}$$

$$A = \frac{\xi A_2 - A_1}{A_2 - A_1}$$

$$B = \frac{\xi - 1}{A_1 - A_2}$$

$$C = \frac{B}{M_1^2 - S^2\,\mathrm{Pr}^2 - S^2\,\mathrm{Pr}}$$

$$C_1 = \frac{K_6K_8 - K_9K_5}{K_4K_8 - K_7K_5}$$

$$C_2 = \frac{K_6K_7 - K_9K_4}{K_5K_7 - K_8K_4}$$

$$D = S/2$$

$$E = S^2/4 + M_1^2$$

$$K_1 = D + \sqrt{E}$$

$$K_2 = D - \sqrt{E}$$

$$K_3 = -C$$

$$K_4 = 1 - \beta_{\mathrm{v}}\mathrm{Kn}K_1$$

$$K_5 = 1 - \beta_{\mathrm{v}}\mathrm{Kn}K_2$$

$$K_6 = K_3 - \frac{A}{M_1^2}\beta_{\mathrm{v}}\mathrm{Kn}K_3S\,\mathrm{Pr}$$

$$K_7 = \exp(K_1) + \beta_{\mathrm{v}}\mathrm{Kn}K_1\exp(K_1)$$

$$K_8 = \exp(K_2) + \beta_{\mathrm{v}}\mathrm{Kn}K_2\exp(K_2)$$

$$K_9 = K_3\exp(S\,\mathrm{Pr}) - \frac{A}{M_1^2} + \beta_{\mathrm{v}}\mathrm{Kn}K_3S\,\mathrm{Pr}\exp(S\,\mathrm{Pr})$$

## List of symbols

| | |
|---|---|
| $b$ | Channel gap |
| $C_{\mathrm{p}}$, $C_{\mathrm{v}}$ | Specific heat for pressure and volume |
| $f_{\mathrm{v}}$, $f_{\mathrm{t}}$ | Coefficient of thermal/tangential momentum accommodation |
| $g$ | Force of gravity |
| $H_0$ | Constant magnetic flux density |
| Kn | Knudsen number $\lambda/b$ |
| In | Fluid–wall interaction parameter $\beta_{\mathrm{t}}/\beta_{\mathrm{v}}$ |
| $M$ | Hartmann number |
| Pr | Prandtl number |
| $Q$ | Dimensionless complex velocity |
| $S$ | Suction/injection parameter |
| $T$ | Temperature of the fluid |
| $T_1$ | Temperature of porous wall at $y = b$ |
| $T_2$ | Temperature of porous wall at $y = 0$ |

$u'$ Main velocity component in $x$-direction
$w'$ Induced velocity component in $z$-direction
$\theta$ Dimensionless temperature
$Q$ Dimensionless volume flow rate

## Greek letters

$\beta$ Coefficient of thermal expansion
$\beta_{\mathrm{h}}$ Hall current parameter
$\beta_{\mathrm{i}}$ Ion-slip parameter
$\alpha_e$ Constant
$\gamma_{\mathrm{s}}$ Ratio of specific heat $C_{\mathrm{p}}/C_{\mathrm{v}}$
$\sigma$ Electrical conductivity of the fluid
$\mu$ Dynamic viscosity
$\xi$ Wall–ambient temperature difference parameter
$\rho$ Density
$\alpha$ Thermal diffusivity
$\lambda$ Molecular mean free path
$\beta_{\mathrm{t}}$ Temperature jump
$\beta_{\mathrm{v}}$ Velocity slip
$\upsilon$ Kinematic viscosity

## Subscripts

$\mathrm{r}$ Reference-state values

**Acknowledgements**
Not applicable.

**Author contributions**
BKJ and PBM contributed to problem formulation, analysis, computation, solution, write-up and mathematical analysis. All authors have read and approved the manuscript.

**Funding**
The authors received no funding on this research.

**Availability of data and materials**
Not applicable.

## Declarations

**Competing interests**
The authors declare that they have no conflict of interest.

Received: 5 April 2021 Accepted: 29 November 2022
Published online: 09 December 2022

**References**

1. Hartmann, J., Hydrodynamics, I.: Theory of the laminar flow of an electrically conducting liquid in a homogeneous magnetic field. Kgl. DanskeVidenskabernesSelskab. Math. Fys. Med. **14**, 1–27 (1937)
2. Jha, B.K., Aina, B.: Magnetohydrodynamic mixed convection flow in vertical microchannel in the presence of induced magnetic field. Int. J. Appl. Mech. Eng. **22**(3), 567–582 (2017)
3. Jha, B.K., Aina, B.: Impact of induced magnetic field on MHD mixed convection flow in vertical micro-channel formed by non-conducting and conducting infinite vertical parallel plates. J. Nanofluids **6**(5), 960–970 (2017)
4. Jha, B.K., Aina, B.: Role of induced magnetic field on MHD natural convection flow in a vertical microchannel formed by two electrically non-conducting infinite vertical parallel plates. Alex. Eng. J. (Facul. Eng. Alex. Univ.) **55**(3), 2087–2097 (2016)
5. Chandran, P., Sacheti, N.C., Singh, A.K.: Hydromagnetic flow and heat transfer past a continuously moving porous boundary. Int. Comm. Heat Mass Transf. **23**, 889–898 (1996)
6. Chandran, P., Sacheti, N.C., Singh, A.K.: Unsteady hydromagnetic free convection flow with heat flux and accelerated boundary motion. J. Phys. Soc. Jpn. **67**, 124–129 (1998)
7. Jha, B.K., Apere, C.: Magnetohydrodynamic Free convection Couette flow with suction and injection. J. Heat Transf. **133**, 092501–092511 (2011)
8. Cowling, T.G.: Magnetohydrodynamics. Interscience Pub, New York (1957)
9. Singh, A.K.: Hall effect on MHD Free-convection flow past an accelerated vertical porous plate. Reidel Publishing Company. Astrophys. Space Sci. **102**, 213–221 (1984)
10. Seth, G.S., Ansari, Md.S.: Magnetohydrodynamics convective flow in a rotation channel with Hall effect. Int. J. Theor. Appl. Mech. **4**(2), 205–222 (2009)

11. Seth, G.S., Singh, J.K.: Mixed convection hydromagnetic flow in a rotating channel with Hall and wall conductance effects. J. Appl. Math. Model. Elsevier. **40**, 2783–2803 (2015)
12. Attia, H.A.: Effect of Hall current on transient hydromagneticCouette-Poiseuille flow of a viscoelastic fluid with heat transfer. Appl. Math. Model. **32**, 375–388 (2008)
13. Jha, B.K., Malgwi, P.B., Aina, B.: Hall effects on MHD natural convection flow in a vertical microchannel. Alex. Eng. J. (Facul. Eng. Alex. Univ.). **1**, 1 (2017). https://doi.org/10.1016/j.aej.2017.01.038
14. Ram, P.C.: Effects of Hall and ion-slip currents on free convective heat generating flow in a rotating fluid. Int. J. Energy Res. **19**, 371 (1995)
15. Ali, A.O., Makinde, O.D., Nkansah-Gyekye, Y.: Effect of Hall current on unsteady MHD coquette flow and heat transfer of nanofluid in a rotating system. Appl. Comput. Math. **4**(4), 232–244 (2015)
16. Makinde, O.D., Iskander, T., Mabood, F., Khan, W.A., Tshehla, M.S.M.H.D.: Coquette-poiseuille flow of variable viscosity nanofluid in a roating permeable channel with Hall effects. J. Mol. Liq. **221**, 778–787 (2016)
17. Veera, K.M., Jyothi, K.: Hall effects on MHD rotating flow of a visco-elastic fluid through a porous medium over an infinite oscillating porous plate with heat source and chemical reaction. Mater. Today: Proc. **5**, 367–380 (2018)
18. Jha, B.K., Apere, C.A.: Combined effect of hall and ion-slip currents on unsteady MHD Couette flows in a rotating system. J. Phys. Soc. Jpn. **79**, 104401 (2010)
19. Jha, B.K., Apere, C.A.: Hall and ion-slip effects on unsteady MHD Couette flow in a rotating system with suction and injection. J. Phys. Soc. Jpn. **80**, 114401 (2011)
20. Mazumder, B.S., Gupta, A.S., Datta, N.: Hall effects on combined free and forced convective hydromagnetic flow through a channel. Int. J. Eng. Sc. **14**, 285–292 (1976)
21. Ghosh, S.K.: MHD rotating flow and heat transfer through a channel with Hall effects. J. Magn. Magn. Mater. **404**, 221–229 (2016)
22. Jha, B.K., Malgwi, P.B.: Computational analysis and heat transfer of MHD transient free convection flow in a vertical microchannel in presence of Hall and ion slip effects. Int. J. Appl. Comput. Math. **8**(156), 1–22 (2022)
23. Seth, G.S., Singh, J.K.: Mixed convection hydromagnetic flow in a rotating channel with Hall and wall conductance effects. Appl. Math. Model. **40**, 2783–2803 (2016)
24. Zhang, L., Bhatti, M.M., Michaelides, E.E., Marin, M., Ellahi, R.: Hybrid nanofluid flow towards an elastic surface with tantalum and nickel nanoparticles, under the influence of an induced magnetic field. Phys. Eur. J. Spec. Top. **231**, 521–533 (2022)
25. Bhatti, M.M., Zeeshan, A., Bashir, F., Sait, S.M., Ellahi, E.: Sinusoidal motion of small particles through Brickman–Forchheimer microchannel filled with Newtonian fluid under electro-osmotic forces. J. Taibah Univ. Sci. **15**(1), 514–529 (2021)
26. Abouelregal, A.E., Marin, M.: The Response of Nanobeams with temperature: dependent properties using state-space method via modified couple stress theory. Symmetry **12**(8), 1276 (2020)
27. Ghita, C., Pop, N., Cioban, H.: Quasi-static behavior as a limit process of a dynamical one for an anisotropic hardening material. Comput. Mater. Sci. **52**(1), 217–225 (2012)
28. Anwar, T., Kumam, P., Baleanu, D., Khan, I., Thounthrong, P.: Radiative heat transfer enhancement in MHD porous channel flow of an Oldroyd –B fluid under generalized conditions. Phys. Scr. **95**, 115211 (2020)
29. Bratu, P., Goanta, A.M., Gragan, N., Vlase, S., Itu, C., Nicolae, G.L., Iacovescu, S.: Dynamic Behavior of the inertial platform related to the research facility building laser and Gamma at ELI-NP Bucharest. Symm. MDPI. **14**(831), 2–18 (2022)
30. Ellahi, R., Vlase, S., Bhhati, M.M.: On the decay of exponential type for the solutions in a dipolar elastic body. J. Taibah Univ. Sci. **14**(1), 534–540 (2020)
31. Jha, B.K., Aina, B., Ajiya, A.T.: Role of suction/injection on MHD natural convection flow in a vertical micro-channel. Int. J. Energy Technol. **7**, 30–39 (2015)
32. Sutton, G.W., Sherman, A.: Engineering Magnetohydrodynamics. McGraw-Hill Book Comp, New York (1965)
33. Eckert, E.R.G., Drake, R.M., Jr.: Analysis of Heat and Mass Transfer, vol. 11. Mcgraw-Hill, New York (1972)
34. Jha, B.K., Samaila, G., Malgwi, P.B.: Adomian Decomposition Method for combined effect of Hall and ion-slip on mixed convection flow of chemically reacting Newtonian fluid in a micro-channel with heat absorption/generation. Int. J. Mod. Phys. C (2020). https://doi.org/10.1142/S0129183120501508


## Publisher's Note